

# The accretion powered spin-up of GRO J1750–27

S.E. Shaw<sup>1</sup>, A.B. Hill<sup>1</sup>, E. Kuulkers<sup>2</sup>, S. Brandt<sup>3</sup>, J. Chenevez<sup>3</sup>, P. Kretschmar<sup>2</sup>

<sup>1</sup>*School of Physics and Astronomy, University of Southampton, Highfield, Southampton, SO17 1BJ, UK.*

<sup>2</sup>*ISOC, ESA/ESAC, Urb. Villafranca del Castillo, PO Box 50727, 28080 Madrid, Spain.*

<sup>3</sup>*National Space Institute, Technical University of Denmark, Juliane Maries Vej 30, 2100 Copenhagen, Denmark.*

Released 2002 Xxxxx XX

## ABSTRACT

The timing properties of the 4.45 s pulsar in the Be X-ray binary system GRO J1750–27 are examined using hard X-ray data from *INTEGRAL* and *Swift* during a Type II outburst observed during 2008. The orbital parameters of the system are measured and agree well with those found during the last known outburst of the system in 1995. Correcting the effects of the doppler shifting of the period, due to the orbital motion of the pulsar, leads to the detection of an intrinsic spin-up that is well described by a simple model including  $\dot{P}$  and  $\ddot{P}$  terms of  $-7.5 \times 10^{-10} \text{ s s}^{-1}$  and  $1 \times 10^{-16} \text{ s s}^{-2}$  respectively. The model is then used to compare the time-resolved variation of the X-ray flux and intrinsic spin-up against the accretion torque model of Ghosh & Lamb (1979); this finds that GRO J1750–27 is likely located 12–22 kpc distant and that the surface magnetic field of the neutron star is  $\sim 2 \times 10^{12} \text{ G}$ . The shape of the pulse and the pulsed fraction shows different behaviour above and below 20 keV indicating that the observed pulsations are the convolution of many complex components.

**Key words:** pulsars: individual: GRO J1750–27 – stars: neutron – X-rays: binaries – X-rays: bursts – ephemerides.

## 1 INTRODUCTION

The number of known high mass X-ray binary systems (HMXB) has expanded in recent years with the advent of hard X-ray satellite telescopes with large fields of view enabling the serendipitous detection of these sources whilst in outburst. In particular the number of HMXB systems comprising a neutron star (NS) with a Be star companion, which in most cases are only seen in brief outbursts following  $\sim$  years of quiescence, has increased to the point where the majority of HMXB known now are such systems (hereafter BeXRB). Be stars are young and hot, with spectral Type B (or O) characterised by Balmer emission lines thought to be associated with circumstellar material shed due to the rapid rotation of the star, which may be near to its disruption speed (see e.g. Porter & Rivinius 2003). The NS, in an elliptical orbit around the star, can accrete matter from an equatorial “decretion disk” that may be formed from the disrupted material, or from a strong stellar wind; this potentially leads to outbursts in X-rays seen at different orbital phases.

The types of outburst can be separated into Type I and Type II (Stella et al. 1986): Type I outbursts are seen to occur around the periastron of the binary orbit (although outbursts are not necessarily seen at every periastron) and are thought to be due to an increase in accretion onto the NS’s surface when it is closest to the Be star where density of matter available is higher; Type II outbursts are much brighter than Type I, do not seem to be correlated with orbital phase and in many cases last for several orbital periods. Pulsed X-rays are often seen from BeXRBs since they contain strongly

magnetised NS; to date there are no known BeXRBs containing a confirmed black hole. Typical pulsar periods,  $P$ , for BeXRBs are in the range 1–100 secs and show a correlation with the binary periods,  $P_{orb}$ , of 10–100 days (Corbet 1986). During Type II bursts the pulsation rate of the pulsar is seen to increase ( $P$  reduces, or frequency  $\nu = 1/P$  increases) suggesting that significant angular momentum transfer from the star to the NS is happening; this phenomena is known as *spin-up*.

The observation of Type II outbursts are particularly interesting for many reasons, especially those where a pulsar can be observed: with luminosities of  $1\text{--}2 \times 10^{38} \text{ ergs s}^{-1}$  they are a factor of  $\sim 10$  brighter than Type I outbursts and should allow good signal to noise even for systems located far away from Earth; the behaviour of the system over at least one full orbital period can be investigated, allowing the orbital characteristics to be inferred from changes in  $P$ ; the matter accretion rate,  $\dot{m}$ , can be studied by relating the spin-up rate,  $\dot{P}$ , of the pulsar to the transfer of angular momentum from the Be star; a period of spin-down of the pulsar towards the end of a large outburst with large spin-up may be indicative that the pulsar has undergone a torque reversal caused by an interaction of the maximally spinning pulsar magnetosphere with the inner accretion disk - this would allow an estimate of the magnetic moment of the NS material to be examined; changes in the orbital phase averaged spectra may allow the Be star environment to be probed.

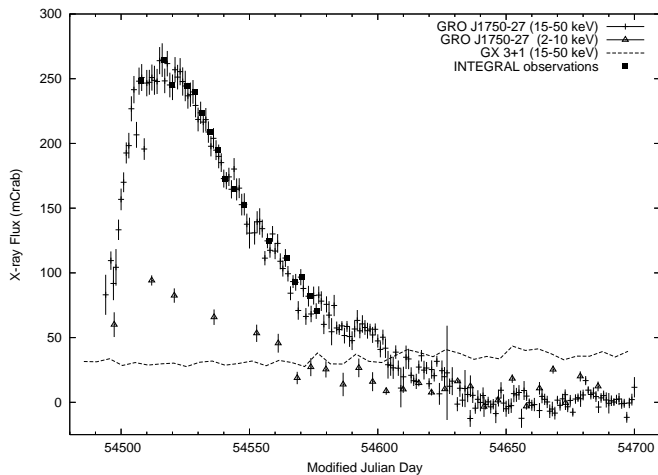


**Figure 1.** GRO J1750–27 X-ray light curves from the *Swift*/BAT transient monitor webpage (<http://swift.gsfc.nasa.gov/docs/swift/results/transients>) and *RXTE*/ASM (<http://xte.mit.edu/ASMLc.html>), shown by vertical crosses and triangles respectively. Dark squares are overlaid on the BAT data to mark where simultaneous observations were made by *INTEGRAL*. The dashed line shows the 15–50 keV flux from the X-ray burster GX 3+1, which is located 18' from GRO J1750–27 (average flux from 5 daily measurements is shown for clarity).

### 1.1 GRO J1750–27

The transient X-ray pulsar GRO J1750–27 (also known as AX J1749.1–2639) was discovered towards the Galactic Centre, by the *CGRO*/BATSE satellite experiment (Scott et al. 1997), following an outburst of 20–70 keV photons over the period MJD 49915–49978 (1995 July 17 – September 18). The BATSE detectors were large wide-angle uncollimated scintillator detectors, hence the outburst was detected only through a pulsed flux with period 4.45 s. Any unpulsed component was not measurable, in the absence of any imaging capability, and formed part of the background signal (along with all other sources in the FoV). The pulsed flux was equivalent to  $\sim 30$  mCrab at its peak. The pulsation was observed to spin-up during the outburst at a rate correlated with the pulsed intensity, reaching  $38 \text{ pHz s}^{-1}$  at the peak of the outburst. A modulation of the period was found to correspond to a 29.8 day orbital period and led Scott et al. (1997) to identify GRO J1750–27 as a BeXRB undergoing a giant (Type II) outburst following the classification of Corbet (1986). Scott et al. (1997) made an estimate of the distance to the source of at least 18 kpc from Earth. Due to the non-imaging nature of the BATSE detectors this measurement is based on an assumed pulsed fraction of 30% for GRO J1750–27.

A second outburst was reported by the *Swift*/BAT transient monitor during an observation starting at 11:26:40 UT on 29th Jan 2008 (MJD 54494). The source was first detected at  $0.031 \pm 0.005 \text{ cts/cm}^2/\text{sec}$  (140 mCrab) in the 15–50 keV energy range of the BAT detector (Krimm et al. 2008). The outburst is shown in Fig. 1 and consists of a sharp rise to the peak flux in  $\sim 30$  days and a slower decay over the following  $\sim 120$  days. The XRT soft X-ray telescope, also onboard *Swift*, has given the currently most accurate position for GRO J1750–27 as  $\text{RA}(2000) = 17^{\text{h}}49^{\text{m}}13^{\text{s}}.1, \text{Dec.}(2000) = -26^{\circ}38'37''.3$  with an uncertainty of  $5''$  (Barthelmy et al. 2008)<sup>1</sup>. Note that the location of

GRO J1750–27 is  $\sim 18'$  from the bright X-ray burster GX 3+1, which requires that observations must be made with instruments with good angular resolution. No optical counterpart brighter than  $R \approx 17$  mag has been reported, although the assumed distance to GRO J1750–27 of 18 kpc and its location of  $(l, b) = (2^{\circ}.4, +0^{\circ}.5)$  place it some distance beyond the Galactic Centre, where optical observations are very difficult due to absorption.

This outburst was also observed by the ESA X-ray/ $\gamma$ -ray satellite *INTEGRAL* during Galactic Bulge monitoring observations (Kuulkers et al. 2008, 2007). The monitoring programme consisted of  $\sim 12$  ksec observations of the Galactic Bulge repeated approximately once per orbital revolution of *INTEGRAL* (the orbital period of *INTEGRAL* is  $\sim 72$  hours) and continued throughout the brightest part of the outburst. Figure 2 shows images taken with the *INTEGRAL* instruments during the peak of the outburst. The JEM-X instrument has finer angular resolution than ISGRI and hence GRO J1750–27 and GX 3+1 are clearly resolved in the low energy image. Nevertheless the two sources are also resolved with ISGRI and, due to the relatively softer spectrum of GX 3+1, GRO J1750–27 is many times brighter at higher energies.

The all sky monitor (ASM) data from the *RXTE* satellite were also inspected to give further coverage of the outburst in the 2–10 keV range (see Fig. 1). Individual ASM observations of GRO J1750–27 have low signal to noise ratios, since the low energy flux was approximately a third of that at higher energies and because the measurements were based on typically only a few hundred seconds of exposure; the observations were also sparsely spaced, with several days between each. This meant that it was necessary to rebin the ASM light curve in order to reduce the uncertainty on the flux measurements to an acceptable level. Finally, the ASM data are affected by contamination from nearby sources, therefore this data was not considered further.

Following the 2008 outburst, the data from *INTEGRAL* and *Swift* were obtained, allowing this fascinating source to be revisited with the advantage of hard X-ray data from simultaneous observations with imaging capability and the benefit of long quasi-simultaneous exposures.

## 2 DATA

### 2.1 INTEGRAL

The *INTEGRAL* satellite is a X-ray/ $\gamma$ -ray observatory that was launched by ESA on 17 October 2002 (Winkler et al. 2003). It was designed with several instruments to offer fine spectroscopy and imaging in the 3 keV–10 MeV range. Two instruments in particular are of interest for this work: above 18 keV, IBIS/ISGRI (Ubertini et al. 2003; Lebrun et al. 2003) provides hard X-ray imaging in a large ( $30^{\circ}$ ) field of view with angular resolution  $\sim 12'$ , point source location accuracy  $\sim 3'$ , sensitivity  $\sim 18$  mCrab for a  $5\sigma$  source seen in an 1.8 ksec observation in the 20–60 keV range (e.g. Kuulkers et al. 2007); the JEM-X soft X-ray monitor (Lund et al. 2003) consists of two identical coded-mask gas detectors sensitive to X-ray photons in the range 3 – 25 keV within a  $5^{\circ}$  field of view and an angular resolution of  $30''$ . Only the JEM-X1 detector was operational during the observations described here.

<sup>1</sup> A position of GRO J1750–27, measured with the *ROSAT* X-ray telescope, is given in Scott et al. (1997) as  $\text{RA} = 17^{\text{h}}49^{\text{m}}12^{\text{s}}.7, \text{Dec.} =$

$-26^{\circ}38'36''$  (J2000) with  $4''$  accuracy, and is cited as *Dennerl and Trumper, A&A, 1997, (in press)*; this paper, or any later one with the same authors, was not found in a literature search.

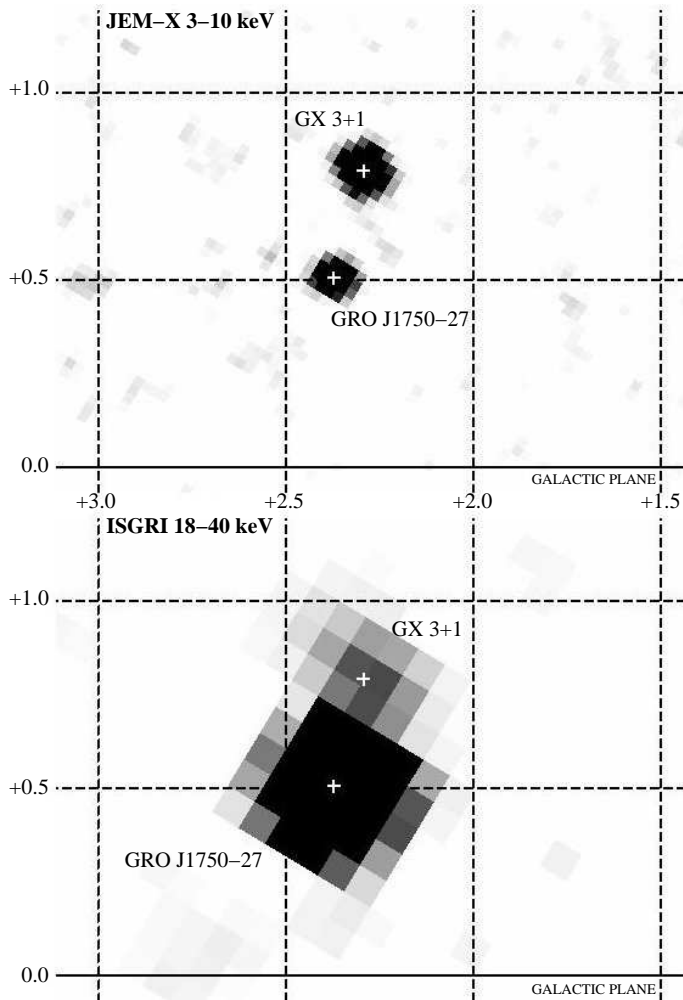


**Figure 2.** Images of the GRO J1750–27 region taken with *INTEGRAL* during revolution 654 (2008 Feb 20; MJD 54516) in the 3–10 keV range with JEM-X1 (top) and 18–40 keV with ISGRI (bottom). The grid shows Galactic coordinates while the grey-scale represents statistical significance. White crosses mark the respective source positions. In the JEM-X image GRO J1750–27 is detected with a peak significance of  $36\sigma$  (corresponding flux 133 mCrab); the peak of GX 3+1 is  $60\sigma$  (235 mCrab). In the ISGRI image GRO J1750–27 is detected with a peak significance of  $117\sigma$  (194 mCrab); the peak of GX 3+1 is  $13\sigma$  (21 mCrab)

*INTEGRAL* makes observations of the Galactic Bulge, approximately every 3 days during the monitoring of the Galactic Bulge (Kuulkers et al. 2007) and is ideal for following up  $\sim$  month long bursts. The coded mask instruments JEM-X and ISGRI have been used to measure the pulsations from GRO J1750–27 in the range 3–70 keV. The data were reduced with the standard Offline Standard Analysis software version 7 (OSA7)<sup>2</sup> provided by the Integral Science Data Centre (ISDC; Courvoisier et al. 2003).

Both ISGRI and JEM-X have good timing characteristics, depending on the brightness of the source in question. Investigation of the 4.45 s pulse from GRO J1750–27 is easily within the capabilities of both *INTEGRAL* instruments.

## 2.2 *Swift*

The *Swift*/BAT instrument on the *Swift* satellite (Gehrels et al. 2004; Barthelmy et al. 2005) is a wide angle coded mask system in a Low Earth Orbit, designed primarily to detect Gamma Ray Bursts (GRB). As such it has a very large field of view, approximately 2 sr, in order to maximise its chance of detecting a randomly occurring GRB. This means that during the course of its normal operations about 15% of the sky is observed and so most areas of the sky have some exposure during each 90 minute orbit. In survey mode, images are produced in histogrammes of approximately 5 minutes length, allowing a light curve of the outburst to be produced with excellent time coverage as seen in Fig. 1. Of course, the survey image histogrammes are of no use for timing investigations on time-scales less than the histogramme duration. However, 1 second count rate data from the whole detector plane is available, which allows strong periodic signals of more than a few seconds length to be observed. In this respect, the observations from BAT are comparable to those made with BATSE in 1995; strong pulsed signals should be detectable, although no measurement of absolute fluxes will be possible from the rate data.

## 3 *INTEGRAL* SPECTRUM AT THE PEAK OF THE OUTBURST

Existing X-ray instruments are unable to use reflection or refraction in optical materials to focus photons with energies more than a few keV (note, however, that several new missions are planned that aim to achieve this in the future with various methods: *Symbol-X*, *NuStar*, *NeXT*, *GRI*). The instruments onboard *INTEGRAL* rely on coded masks to cast a shadow on a position sensitive detector, which can then be used to reconstruct the direction of the incident light. Some contamination of the flux measurement for a particular object is therefore unavoidable in observations of fields containing many sources. Spectral analyses of objects in the Galactic Centre will therefore be challenging and especially so for GRO J1750–27 given its proximity to, and the relative brightness of, GX 3+1 (see Fig. 2).

In particular, the OSA7 tools for spectral analysis with JEM-X are optimised for a single on-axis source and for fields containing many sources it is recommended to make spectra from fluxes taken from images made in discrete energy ranges<sup>3</sup>. This method is thought to be more immune to contamination of the spectra than the standard method, although it is not practical to make images in bands less than  $\sim$  1–2 keV wide. A comparison of spectra made by both methods, for the peak of the outburst during revolution 654, showed that they were consistent above 5 keV; at lower energies there was a clear overestimate in the flux using the standard OSA7 spectral extraction method.

For higher energy spectral analysis with ISGRI the detrimental effects of other sources are somewhat reduced since, in revolution 654, GRO J1750–27 is brighter than GX 3+1 above 18 keV by about a factor of ten and is also the brightest source in the whole field of view by a factor of two.

The broadband spectrum during the peak of the outburst was therefore calculated in the 5–70 keV range and fit with a cut-off power law:

<sup>2</sup> OSA7 is available from the ISDC at <http://isdc.unige.ch>

<sup>3</sup> See *Known Issues* in the JEM-X analysis cookbook at <http://isdc.unige.ch/?Soft+download>

$$A(E) = K \left( \frac{E}{1 \text{ keV}} \right)^{-\Gamma} e^{(-E/E_c)} \quad (1)$$

In order to investigate the energy spectrum of GRO J1750–27, the data from JEM-X1 and ISGRI were fitted simultaneously with a phenomenological model, namely a cut-off power-law function. The spectrum can be seen in Fig. 3. Systematics of 3% were added to JEM-X and 2% added to ISGRI and an inter-instrument calibration factor, defined as a factor applied to the ISGRI spectral response with JEM-X held constant, was also included as a free parameter. This gave a chi-squared value of  $\chi^2/dof = 28.6/22$  and returned values of  $\Gamma = -0.15 \pm 0.3$  and  $E_c = 6.0^{+0.5}_{-0.4}$  keV respectively (90% confidence) and an instrument calibration factor of 1.49. Assuming that most of the energy output of the source is in the range 0.1–100 keV gives a total flux of  $6.5 \times 10^{-9}$  ergs  $\text{cm}^{-2} \text{s}^{-1}$ , although the uncertainty on this is  $\pm 30\%$  due to the variation on the measurement of  $\Gamma$  alone.

A physical model, ascribing the spectral behaviour of the source to the inverse Compton scattering of soft photons by a thermal plasma of electrons, was also fitted to the data. The COMPTT model of Titarchuk (1994) returned a reduced chi-squared value of 1.24 and the following values: the plasma temperature  $4.6 \pm 0.1$  keV; the plasma optical depth  $6.4^{+0.9}_{-0.7}$ ; the soft photon temperature was fixed at 0.1 keV as it lies far outside of the range covered by our spectral data. The inter-instrument calibration factor was 1.40. This model follows essentially the same form as the cut-off power-law, as can be seen in Fig. 3, and suggests that the X-ray spectrum is due to the scattering of soft X-ray photons in an optically thick plasma.

In both cases, the calibration factor returned was not equal to unity. This shows that there are some systematic effects in the spectrum that are not fully understood when dealing with moderately bright sources in crowded fields. Since the fields of view of ISGRI and JEM-X are not the same size, the backgrounds of both instruments will be dependent on different objects. The objects contained in both fields of view will also not have the same effects on each instrument, due to the large range of the X-ray spectra of the objects in the Galactic Bulge; each source may have a different relative brightness to GRO J1750–27 in the energy bands of the two instruments, and will therefore be of changing importance to both background estimations.

The detailed analysis of the GRO J1750–27 spectrum is clearly complicated even when the source is at its brightest; understanding the instruments' spectral response during the observations, and hence the spectral behaviour of GRO J1750–27 throughout the outburst and its variation with pulsar phase, will be the subject of future work. In order to investigate the spectral behaviour, without model dependent spectral fits, simple spectral hardness ratios have been calculated from the total count rate fluxes measured by *INTEGRAL* during the outburst:

$$h = \frac{(F_I - F_J)}{(F_I + F_J)} \quad (2)$$

where  $F_I$  is the 20–50 keV ISGRI count rate and  $F_J$  is the 5–20 keV JEM-X count rate. Figure 4 shows the time evolution of the broad band spectral hardness in the 5–20 and 20–50 keV ranges for the total (pulsed+unpulsed) data. There is a gradual softening of the total flux from GRO J1750–27 during the outburst, with some indications of more complex variability.

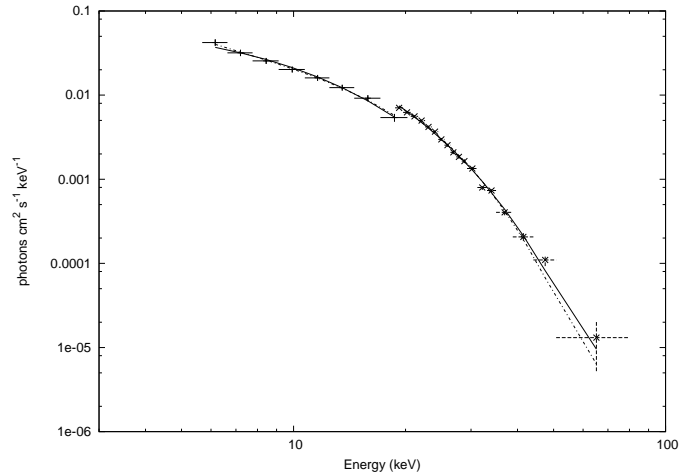


**Figure 3.** The *INTEGRAL* spectrum of GRO J1750–27 during the peak of the outburst in revolution 654. Measurements with JEM-X1 cover the 3–20 keV range (vertical crosses), whilst ISGRI data is taken from 18–50 keV (diagonal crosses). The lines show models which have been simultaneously fitted to both data sets as described in section 3: comptonisation (continuous line); cut-off power-law (dashed-dotted line).

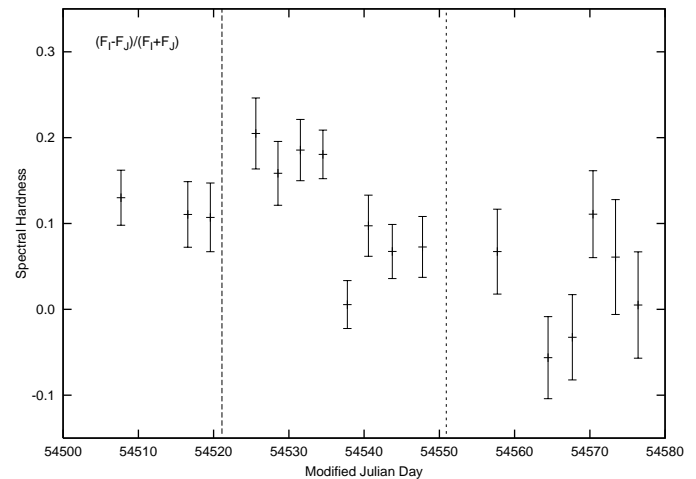


**Figure 4.** *INTEGRAL* measurements of the hardness ratio,  $\frac{(F_I - F_J)}{(F_I + F_J)}$ , where  $F_I$  is the 20–50 keV ISGRI count rate and  $F_J$  is the 5–20 keV JEM-X count rate. The dashed vertical lines show the times of periastron of the GRO J1750–27 system.

## 4 HARD X-RAY TIMING ANALYSIS

### 4.1 ISGRI pulsation detection at 18–40 keV

The OSA7 tools *ii.light* and *barycent* were used to create 18–40 keV light curves, with 0.5 s binning, and to correct the time stamps of the results for the orbital motion of the *INTEGRAL* satellite, for each set of Galactic Bulge monitoring observations.

The ISGRI light curves analysed here are made from several fixed pointings separated by slews and, as is common in high-energy astrophysics observational analysis, may contain irregularly distributed time data affected by telemetry gaps etc. Therefore the Lomb-Scargle method (Lomb 1976; Scargle 1982), which is robust against these effects, is used to search for periodic signals. The error on the angular frequency of any detected pulsation is given by the formulations of Horne & Baliunas (1986):

$$\delta\omega = \frac{3\pi\sigma_N}{2\sqrt{NTA}} \quad (3)$$

where the amplitude  $A$  is calculated thus,

$$A = 2\sqrt{\frac{z_0\sigma_s^2}{N}} \quad (4)$$

$\sigma_N$  is the standard deviation of the noise in the lightcurve, estimated to be the same as the standard deviation of the lightcurve,  $\sigma_s$ , for a weak pulsed signal;  $z_0$  is the power of the pulsation from the periodogram;  $N$  is the number of data points;  $T$  is the total length of the data set.

In each of the 17 Galactic Bulge monitoring observations the Lomb-Scargle periodograms showed a significant peak at a frequency of  $\nu \sim 0.22$  Hz. This corresponds to a period of  $\sim 4.45$  s which is in agreement with the observed spin period identified by Scott et al. (1997). Table 1 lists the detected pulse period and the associated error for each observation. The ISGRI data clearly show periodic signals which can be measured with very high accuracies, typically  $\sim$  few parts in  $10^5$ .

## 4.2 ISGRI measurements of pulsar spin-up

The GRO J1750–27 pulse period,  $P$ , as a function of observation time is shown in Fig. 5 and clearly indicates that the observed spin period evolves with time. While the oscillatory motion may be explained by a doppler shifting of the spin-period by the binary orbit of the system there is also an additional component resulting in an intrinsic spin-up of the pulsar.

The observed data was fit with a simple spin-up model for the pulsar given by:

$$P(t) = P(t_0) + \dot{P}(t - t_0) - \frac{\ddot{P}(t - t_0)^2}{2} \quad (5)$$

This model is convolved with a standard orbital model assuming the orbital parameters measured by Scott et al. (1997), excluding the orbital period. This combined model when fit to the data resulted in a chi-square value of  $\chi^2/\text{dof} = 12.78/13$ . An orbital period of  $29.806 \pm 0.001$  days was found which is compatible with that previously observed; there is also a clear measurement of  $\dot{P}$  and  $\ddot{P}$ . The details of the fit parameters and the orbital parameters of Scott et al. (1997) are given in Table 2. The resultant best fit model is presented by the solid line in Figure 5.

Refitting the data without assuming any of the parameters of Scott et al. (1997) yields an acceptable fit. However, whilst the orbital parameters are compatible with the previous observation they have larger associated errors; therefore the preferred fit is based on the original parameters. Removing the  $\dot{P}$  parameter results in an unacceptable fit,  $\chi^2/\text{dof} = 50.04/14$ . An *fstest* on these fit results shows that the addition of  $\dot{P}$  is highly significant, with a chance improvement probability of only  $3 \times 10^{-5}$ . Removing both the  $\dot{P}$  and  $\ddot{P}$  terms returns an even poorer fit by many orders of magnitude:  $\chi^2/\text{dof} \sim 6000/15$ . Hence the intrinsic spin-up model of equation 5 is determined with a very high level of confidence.

## 4.3 Pulsation measurements with JEM-X

Following similar methods to the ISGRI analysis, data from the soft X-ray monitor onboard *INTEGRAL*, JEM-X1, were reduced with *OSA7* for a broad 5–20 keV energy band. The analysis of the JEM-X data returned values of  $P$  consistent with the ISGRI results for all contemporaneous observations, albeit at lower statistical significance. In several of the earlier observations significant power was

**Table 1.** 18–40 keV pulsations detected from *INTEGRAL*/ISGRI observations of GRO J1750–27.

Revolution	MJD	Exposure (ks)	Period (s)	$\Delta$ Period (s)
0651	54507.687	5	4.4545	0.0002
0654	54516.572	12	4.45270	0.00003
0655	54519.562	12	4.45175	0.00004
0657	54525.545	7	4.45315	0.00004
0658	54528.538	12	4.45351	0.00006
0659	54531.530	13	4.45335	0.00007
0660	54534.522	12	4.4532	0.0001
0661	54537.773	12	4.4528	0.0002
0662	54540.509	10	4.45208	0.00014
0663	54543.752	12	4.45180	0.00010
0664	54547.759	14	4.45058	0.00007
0667	54557.708	12	4.45208	0.00007
0670	54564.432	24	4.45198	0.00002
0671	54567.682	12	4.45169	0.00006
0672	54570.413	10	4.45130	0.00010
0673	54573.403	11	4.45081	0.00008
0674	54576.395	12	4.44996	0.00007

**Table 2.** The orbital parameters for GRO J1750–27 derived from Scott et al. (1997) and from the analysis of ISGRI 20–40 keV data.

Scott et al. (1997)		
Orbital period	$P_{orb}$	$29.817 \pm 0.009$ days
Projected semimajor axis	$a_r \sin i$	$101.8 \pm 0.5$ lt-s
Eccentricity	$e$	$0.360 \pm 0.002$
Longitude of periastron	$\omega$	$206^\circ.3 \pm 0^\circ.3$
Orbital epoch	$T_{periastron}$	MJD $49931.02 \pm 0.01$
This work		
Orbital period	$P_{orb}$	$29.806 \pm 0.001$ days
Spin period (@ MJD 54516.635)	$P$	$4.45349 \pm 0.00002$ days
1 <sup>st</sup> derivative of $P$	$\dot{P}$	$-7.5 \pm 0.3 \times 10^{-10}$ s s <sup>-1</sup>
2 <sup>nd</sup> derivative of $P$	$\ddot{P}$	$1.0 \pm 0.1 \times 10^{-16}$ s s <sup>-2</sup>

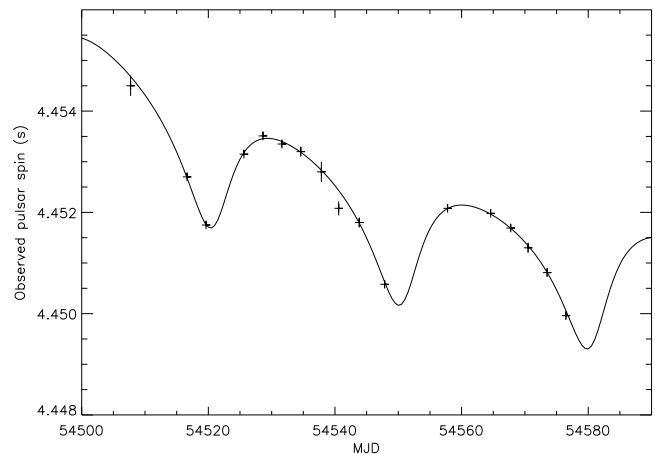


**Figure 5.** GRO J1750–27 orbital solution based on ISGRI measurements (crosses). Note in most cases the error bars on the period are much smaller than the size of the crosses.

also seen at  $\sim 2.22$  s, corresponding to half of the ISGRI period. Inspection of the phase-folded JEM-X light curves showed that below 20 keV the pulse amplitude was weaker and in some cases showed a double peaked profile. This is investigated in section 4.5

#### 4.4 Searching the *Swift*/BAT data for a periodic signal

The  $\sim 2$  sr field of view of BAT means that many observations are made of the source location; if suitable power spectra can be produced then the spin history will be well covered in time. Since the survey mode data, from which images can be produced, are integrated over  $\sim 5$  mins they are not usable for timing studies of GRO J1750–27. The only BAT data with suitable time resolution is the detector plane count-rate, in which the total flux on the whole detector plane is read every second. Since no positional information is available from these data, any pulsed signal from GRO J1750–27 is contaminated by the signals from all other sources in the very large field of view. This can be effectively considered as an increase in the background noise which will appear non-statistical. No time dependent background correction is available for the count-rate data in the current *Swift* standard analysis and consequently it has not been possible to extract reliable pulsed fluxes. The BAT does, however, have the advantage of many observations of GRO J1750–27 throughout the outburst.

Data were obtained for all pointings between MJD 54480 and 54640 (2008 January 15 and June 23) where the position of GRO J1750–27 was within  $30^\circ$  of the pointing direction. This was to obtain a sub-set of data not too badly affected by noise towards the edge of the detector plane and so that the source was detected with a reasonable sensitivity. The data were broken up into 50 ks segments, which were defined consecutively from the start of the observation, and were each searched for a periodic signal. Due to the low Earth orbit of *Swift* and its pointing strategy the data are generally arranged in a few short sections of  $\sim 1000$  seconds duration within the time bin.

To improve the chances of detecting the pulsar spin period a Bayesian statistical approach is applied to the data set. The generalised Lomb-Scargle periodogram method of Bretthorst (2001) is used with the period range of interest restricted to the narrow range 4.445–4.460 s i.e. tightly bounding the periodicity detected by ISGRI.

Figure 6 shows the resulting periodograms displayed as a function of time and coloured for the probability density at each period. The highest probability density corresponds to periods which are consistent with the ISGRI measured pulses and the fitted period model; this is shown by the central dashed line in Figure 6. Also evident are side lobes of lower probability which follow the same time evolution; these are offset from the main track by integer units of a constant,  $k = \pm 3.4$  ms. If this effect is caused by the beating of the pulsation with another periodic signal is given by the following:

$$\frac{1}{P_{beat}} = \frac{1}{P} - \frac{1}{P+k} \quad (6)$$

Inserting  $P = 4.450$  s gives  $P_{beat} \sim 97$  minutes, which corresponds approximately to the orbital period of the *Swift* satellite. The secondary tracks are therefore very likely to be due to aliasing with subtle effects on the count-rate or spacecraft orientation occurring on the *Swift* geo-orbital period.

Figure 6 shows that ISGRI derived orbital solution is valid throughout the outburst and can be reliably extrapolated to times after the ISGRI observations ended at MJD 54576. The first BAT survey mode data available for the outburst, as shown in Fig. 1,

is on MJD 54494; detector plane rate data is available before this time, although there does not seem to be any strong evidence for a pulsed signal before  $\sim$  MJD 54490.

As  $\dot{P}$  is a tracer of the mass accretion rate,  $\ddot{P}$  can be used as an indicator of how  $\dot{m}$  changes i.e. the rate at which the mass contained within the accretion disc is being exhausted. Consequently, we can define a simple timescale for the survival of the accretion disc,  $\tau$ , as:

$$\tau = -\frac{\dot{P}}{\ddot{P}} \quad (7)$$

This gives  $\tau = 87 \pm 9$  days based upon the ISGRI measurements shown in Table 2. Extrapolating from the time of peak of the outburst this implies that the outburst should end at  $\sim$ MJD 54611.

#### 4.5 Pulse Profile

The shape of the pulse profiles has been measured over the 5–50 keV range with *INTEGRAL*. As seen in section 4.1 the ISGRI timing results are highly accurate with strong power spectra leading to uncertainties on  $P$  of typically  $200 \mu\text{s}$ . Phase diagrams for the pulsar were made from the ISGRI 20–50 keV data from each revolution by folding on the measured period. An offset was then added to the phase diagram so that the brightest phase bin was centred at phase = 0. The period and epoch defined by ISGRI were then used to fold the JEM-X data in 5–25 keV band in order to make comparable phase diagrams, which are shown in Figure 7.

In general the shapes of the pulses seem to be more complex in shape below 20 keV than they are above 20 keV; below 20 keV, there are clear signs of a double peaked pulse profile. A secondary peak, approximately 50% the size of the primary peak, is especially noticeable in revolutions 654 and 655. In the same revolutions the pulse profile also shows signs of a secondary peak above 20 keV, although its relative size is much reduced. The pulse appears weak in revolutions 660–662; in revolution 660 the pulse can barely be detected at all. It is interesting to note that these three observations straddle the apastron of the system, when the separation between Be star and NS is largest and presumably the rate of accretion from any circumstellar material would be at a minimum. The suggestion is therefore that there is a connection between the orbital phase and the strength or shape of the pulsation. However, the observations of revolutions 670–672 are also taken at approximately the same orbital phases, and here a very clear sinusoidal pulse is visible. Unfortunately, determining any connection with the behaviour of GRO J1750–27 and the orbital phase would certainly require observing an outburst over a larger number of orbital cycles and is not possible here. The variation in the pulse shapes from observation to observation show that it would not be appropriate to attempt to improve the signal to noise by making an average of many pulses.

#### 4.6 Pulsed Fraction

The evolution of the pulsed fraction as defined in Bildsten et al. (1997), namely the ratio of the integrated peak-trough flux divided by the mean (pulsed+unpulsed) flux, is shown in Fig. 8. The pulse profiles in Fig. 7 were rebinned by a factor of two in order to calculate these values. The pulsed fraction in the 5–20 keV band varies between 5–15 %; above 20 keV the pulsed fraction is higher and has a larger variation,  $\sim 10$ –40 %. Both the 5–20 keV and 20–50 keV data show similar evolutions of the pulsed fraction with a slow rise in the first few observations, followed by a minimum

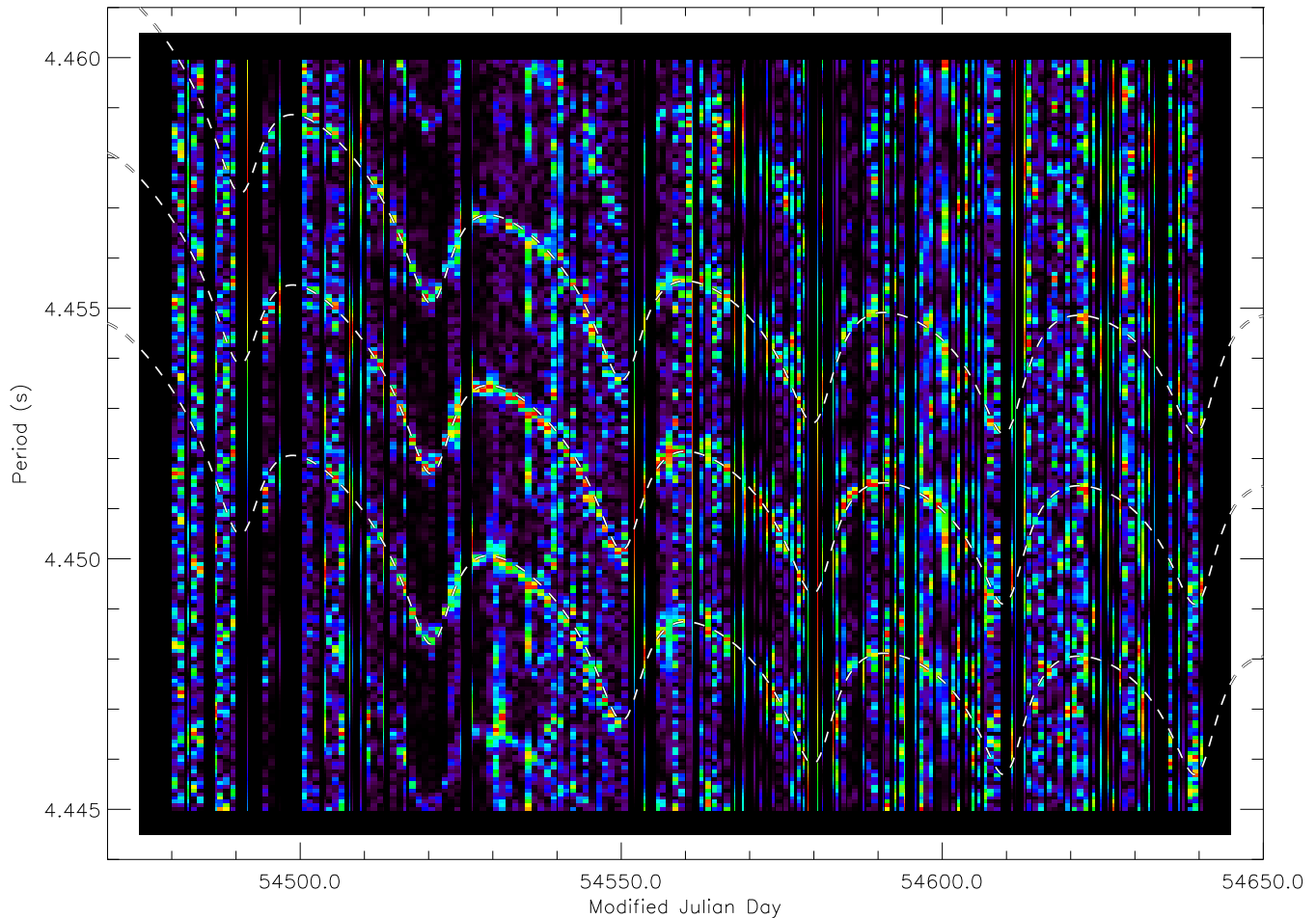


**Figure 6.** Dynamic periodogramme measured from 50 ksec sections of *Swift*/BAT detector plane count-rate data for the period MJD 54480–54640 (2008 January 15 – June 23) using the Bayesian analysis method outlined in section 4.4. Pulsation probability is represented with a rainbow colour scale with red representing high confidence of a pulsed signal. The central dashed line shows the orbital solution for the pulse variation measured from the ISGRI data (see section 4.1); the upper and lower dashed lines show the model offset by  $\pm 3.4$  ms. The ISGRI orbital model is in very good agreement with the BAT observations, no scaling or normalising of the ISGRI model has been performed. The offset lines agree with the secondary tracks caused by the aliasing of the pulsed signal with the *Swift* spacecraft orbital period.

at revolution 660. In the 5–20 keV band the pulsed fraction seems to recover quickly to around 12 % in revolution 661 and remains approximately constant from then on; this behaviour is quite different above 20 keV, where the pulsed fraction increases slowly from revolution 661 towards the end of the *INTEGRAL* observations.

## 5 DISCUSSION

The pulsar spin-up and orbital parameters of the BeXRB system GRO J1750–27 have been measured to a high precision from hard X-ray observations with *INTEGRAL* and *Swift* (see Table 2). These were found to be in good agreement with the measurements made by Scott et al. (1997) during the previous known outburst from this system in 1995. Assuming a cut-off power law model to describe the spectrum measured with *INTEGRAL* during the peak of the outburst and extrapolating to 0.1–100 keV gives a total flux from the source of  $6.5 \times 10^{-9}$  ergs  $\text{cm}^{-2}$   $\text{s}^{-1}$ ; assuming that during the peak of the outburst the source is radiating at the Eddington luminosity,  $1.8 \times 10^{38}$  ergs  $\text{s}^{-1}$ , puts an estimate on the distance to the source of

around 15 kpc although this value is very uncertain due to the difficulties measuring and then extrapolating the 5–50 keV spectrum and also assumes spherically symmetric accretion onto the NS.

The observed rapid spin-up of X-ray pulsars in outburst is proportional to the rate of angular momentum transfer from the donor star, which is in turn proportional to the rate of matter transferred to the NS through accretion, and also proportional to the X-ray luminosity of the source (e.g Pringle & Rees 1972). In binary systems with an accretion disk, the rate of spin-up is curtailed by the threading of the accretion disk with magnetic field lines from the NS, which causes a torque to be imparted to the NS and acts to reduce the rate of spin-up. This model was first proposed by Ghosh & Lamb (1979) and although other more detailed models have been proposed (e.g Wang 1987, 1995) they are largely consistent with the original. Ghosh & Lamb (1979) suggest that for a NS with radius  $1 \times 10^6$  cm and given magnetic moment,  $\mu$ , the value of  $\dot{P}$  is dependent only on the quantity  $PL^{3/7}$ , where  $L$  is the bolometric luminosity of the source. The changing luminosity can be estimated from the *Swift*/BAT light curve (fig 1), which has ex-

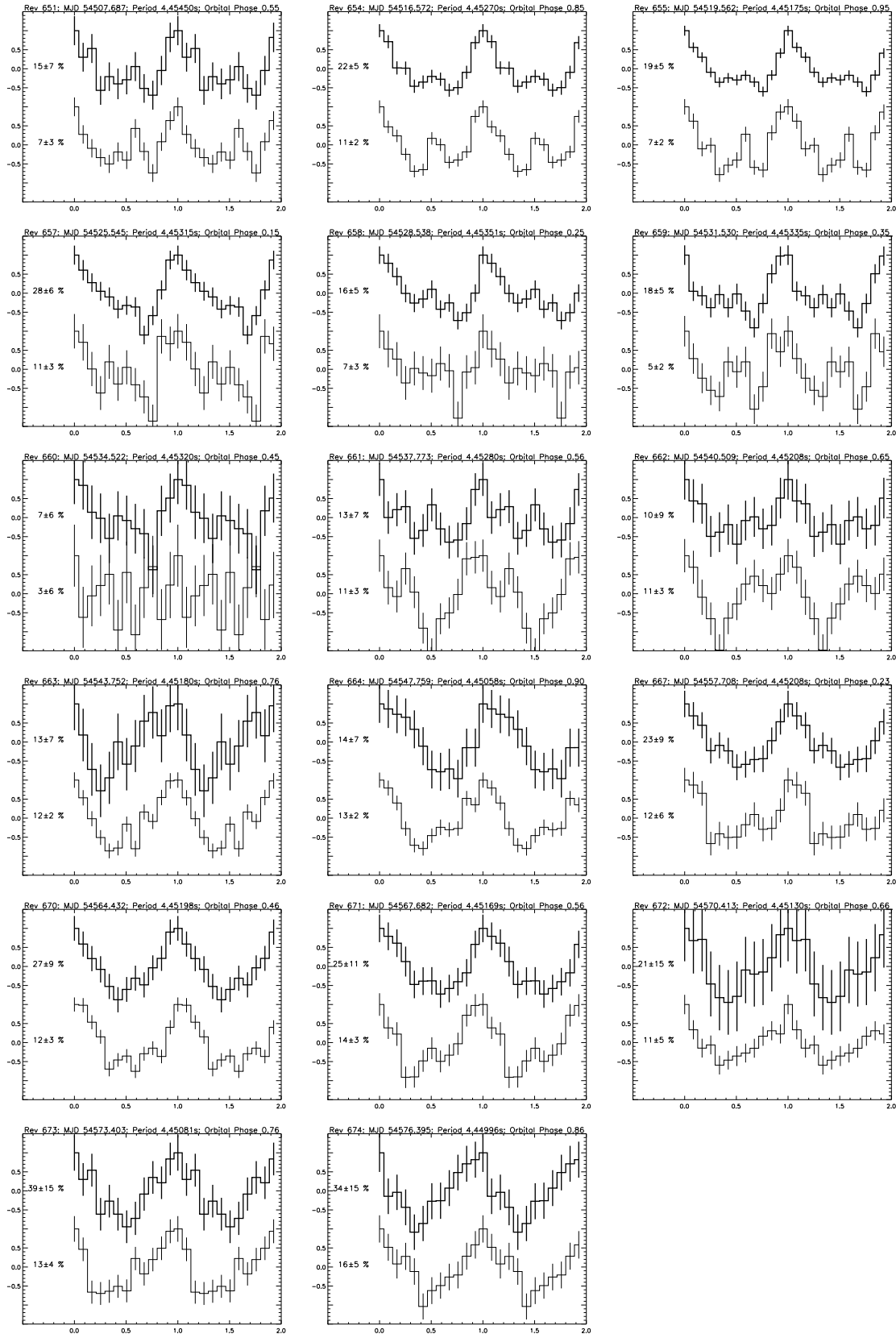


**Figure 7.** Relative pulse profile diagrammes for different *INTEGRAL* observations of the 2008 outburst of GRO J1750–27: ISGRI 20–50 keV (top, thickest); JEM-X 5–20 keV (bottom, thinnest). The data were folded on the periods listed in Table 1 and are indicated at the top of each plot along with the start date of the observation and the estimated orbital phase (0 = periastron) at that date. For clarity, the profiles are repeated for two phases. The numbers to the left of the profiles indicate the pulsed fraction and uncertainty.



cellent time coverage of the outburst and consists of average flux measurements taken daily.

The BAT count rate was converted into  $\text{erg cm}^{-2}\text{s}^{-1}$  by comparing with the many *Swift*/BAT observations of the Crab Nebula; the average Crab Nebula count rate in 15–50 keV is 0.22 counts  $\text{cm}^{-2}\text{s}^{-1}$ . In the same energy range, the Crab nebula was estimated to be  $1.6 \times 10^{-8} \text{ erg cm}^{-2}\text{s}^{-1}$ , assuming a photon spectrum of  $dN/dE = 10E^{-2.05}$  (Zombeck 2007). In order to find a bolometric luminosity, it is assumed that most of the energy output from GRO J1750–27 is in the range 0.1–100 keV. The spectrum described in section 3 returns a 15–50 keV flux that is approximately a factor of 3 less than the total flux. Hence the BAT count rates can be converted to total energy output in ergs by scaling by the factor  $3 \times (1.6 \times 10^{-8}/0.22)$ . This leads to a simple expression for the luminosity in units of  $10^{37} \text{ ergs s}^{-1}$ ,  $L \approx 2.6F_{\text{BAT}}d^2$ , where  $F_{\text{BAT}}$  is the BAT measured count rate in the 15–50 keV band and  $d$  is the distance to the source in kpc.

The intrinsic spin-up model (Equation 5) was then used to calculate  $\dot{P}$  for the duration of each daily BAT measurement. The results, calculated for various values of  $d$ , are presented in Fig. 9 against the models of Ghosh & Lamb (1979) for a  $1.4 M_{\odot}$  NS with a radius of  $10^6$  cm and various values of  $\mu$ . Several results are shown for the BAT data scaled for different distances.

It can clearly be seen in Fig. 9 that from the peak of the outburst, when  $PL^{3/7}$  is highest, that the BAT data show a slope that closely matches the gradient of the model, before turning over when the magnetic torque is expected to start to brake the pulsar. This requires confidence in the shape of the BAT light curve; a similar effect could be caused if there was an over estimation of the flux from GRO J1750–27 towards the end of the outburst. In section 4.4, the spin-up of the pulsar was found to end at MJD 54611, which is when the 15–50 keV flux from GRO J1750–27 is approximately equal to that from GX 3 + 1 (Fig. 1). The separation of the two sources is  $18'$ , slightly less than the FWHM of the BAT angular resolution of  $22'$  (Barthelmy et al. 2005). Assuming a Gaussian point spread function, where the FWHM is equal to  $2.35\sigma$ , the maximum possible contamination of a measured flux caused by an equally bright source located  $18'$  away is  $\sim 5\%$ . If the measured flux from GRO J1750–27 was over-estimated by this amount it would have a negligible effect on the appearance of the data in Fig. 9 - equivalent to causing a value of  $\log(PL^{3/7}) = 1$  to be changed to  $\sim 0.97$ . In addition, the flux from GX 3 + 1 shown in Fig. 1 remains reasonably constant throughout the outburst and no significant correlation was found between the two light curves. Finally, the ability of the BAT `batcelldetect` software, which is used to prepare the transient monitor light curves, to successfully resolve two sources is thought to be accurate where the separation is more than  $10'$  (Krimm, private communication). Therefore any contamination of the GRO J1750–27 flux is likely to be considerably less than 5%.

The value of  $\mu$  which seems to most closely resemble the model is  $\sim 3 \times 10^{30} \text{ G cm}^3$ , corresponding to a magnetic field at the surface of the NS of  $\sim 2 \times 10^{12} \text{ G}$ . Fig. 9 suggests a distance to GRO J1750–27 of around 16 kpc. However, estimating the distance from this model is uncertain due to the difficulties in estimating the spectrum of GRO J1750–27 and the crude scaling of the flux values against the Crab Nebula, which is quite a different object spectrally to GRO J1750–27; a variation in the bolometric correction of a factor of 2, for example, would lead to a change in the distances by a factor of  $\sqrt{2}$ . Nevertheless, this makes it very likely that the object is located some distance beyond the Galactic centre (approx 8.5 kpc from Earth), which is reinforced by the non-detection of any optical counterpart. A value of 30 kpc, which would put

GRO J1750–27 outside the Galaxy, seems unlikely; additionally, a distance greater than 16 kpc would make GRO J1750–27 the furthest HMXB yet detected by *INTEGRAL* (Bodaghee et al. 2007). A reasonable estimate on the range of acceptable distances measured here is therefore 12–22 kpc. HMXBs are relatively young systems that should be found near to their birth places in star formation regions in the spiral arms of the Galaxy; the 4-arm spiral model of Russeil (2003) gives distances to the Perseus ( $\sim 14$  kpc) and Cygnus ( $\sim 16$  kpc) arms that are within the range measured here. Note that the 18 kpc distance lower limit estimated by Scott et al. (1997) was based on an assumed pulsed fraction of 30%; if the pulsed fraction during the 1995 outburst was  $\sim 15\%$ , as measured in section 4.6, their distance would be reduced to  $> 13$  kpc. Whilst the distance estimates are uncertain, the change in  $\dot{P}$  due to the accretion torque predicted by Ghosh & Lamb (1979) seems to agree with the data.

The strong magnetic field estimated at  $\sim 2 \times 10^{12} \text{ G}$  opens the possibility to observe a Cyclotron Resonance Scattering Feature (CRSF) in the X-ray spectrum of GRO J1750–27. To date CRSFs have been detected from 16 accreting pulsars (Schönherr et al. 2007) and in V 0332+53 have also been observed to evolve with time (Kreykenbohm et al. 2005; Mowlavi et al. 2006; Tsygankov et al. 2006). In the case of GRO J1750–27 the fundamental CRSF should be centred near to 22 keV; this would be challenging to observe with *INTEGRAL* as the peak would lie near to the boundaries of the ISGRI and JEM-X sensitivities and the peak flux from GRO J1750–27 is about a factor of 5 less than for V 0332+53, but is something that will be investigated in the future. Similarly, the monitoring capabilities of BAT could allow very detailed measurements of the evolution of CRSFs during a long outburst, if the sensitivity in narrow spectral bins was optimised.

It is interesting that in both 5–20 and 20–50 keV energy bands the pulsed fraction maxima during the early part of the outburst appear near the periastron of the binary system, and that the minima are near apastron; however, the connection between the bands is broken in *INTEGRAL* revolutions 661–664 and in the following orbit no rise and fall of the pulsed fraction is visible within the error bars. Unfortunately, even if there were some correlation of the behaviour of GRO J1750–27 with the orbital period it would be very difficult to confirm it with observations that sparsely cover only a few orbital phases. The behaviour of the pulsed fraction with the overall brightness of the source is shown in figure 10. Above 20 keV there is a clear evolution of the pulsed fraction with flux, with opposite behaviour below and above 30 cps: at the beginning of the outburst (right of figure 10) the pulsed fraction decreases proportionally as the source dims towards 30 cps; below 30 cps the pulsed fraction increases with decreasing flux. Note that the first point above 30 cps is the one taken during revolution 660, where the pulsation was at its weakest in 20–50 keV and not measurable in 5–10 keV (see figure 7). This also seems to coincide with a large drop in the average 20–50 keV flux between revolutions 660 and 661. The same effect is not visible in the lower energy band which, except for a minimum again during revolution 660, shows a slow increase in the pulsed fraction with reducing count rate.

The different behaviour above and below 20 keV rules out the attenuation of the pulsed flux by some intervening material that slowly accumulates and then dissipates; in this scenario the lower energy X-rays would show at least as strong an effect as at high energies. Work continues to investigate these effects with fine resolution temporal-spectral analysis.

On their own, the pulse period measurements made using the BAT non-imaged count-rate data would be difficult to interpret be-

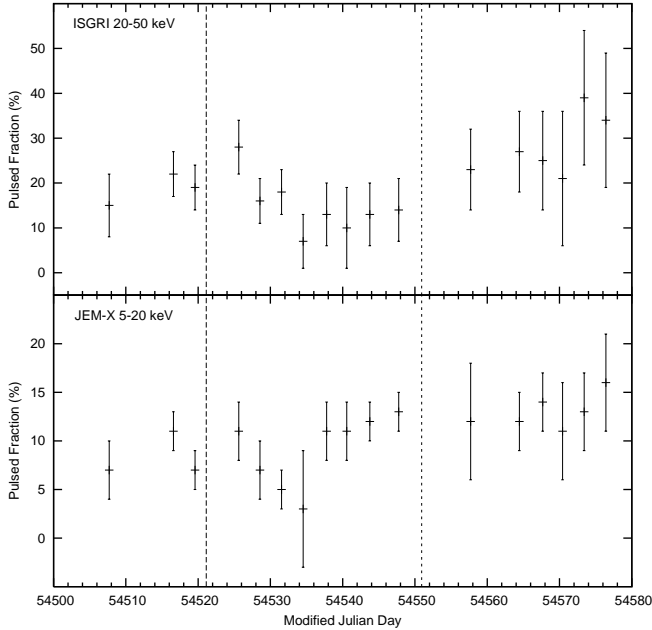


**Figure 8.** *INTEGRAL* measurements of the pulsed fraction during the outburst. The dashed vertical lines show the times of periastron of the GRO J1750–27 system.

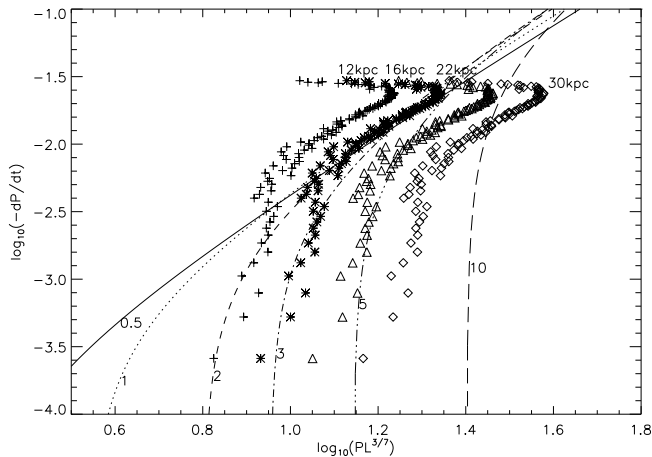


**Figure 9.** Plot of  $\dot{P}$ , taken from the spin-up model measured based on the *INTEGRAL* data (section 4.2), against the quantity  $PL^{3/7}$  derived from the 15–50 keV *Swift*/BAT count rates scaled for various distances (points). Each series of points is labelled with the distance, in kpc, used to estimate the luminosity from the *Swift*/BAT count rates. The different lines show the model of Ghosh & Lamb (1979) for a  $1.4 M_{\odot}$ ,  $10^6$  cm NS for various values of the neutron star magnetic moment,  $\mu$  (indicated towards the bottom of each line). The units of  $\dot{P}$ ,  $P$ ,  $L$  and  $\mu$  are  $\text{s yr}^{-1}$ , s,  $10^{37}$  ergs  $\text{s}^{-1}$  and  $10^{30}$  G  $\text{cm}^3$  respectively. The value of  $\log_{10}(PL^{3/7})$  for a 4.45 s pulsar emitting at the Eddington luminosity of  $\sim 2 \times 10^{38}$  erg  $\text{s}^{-1}$  is approximately 1.2; a value of 1.4 is approximately 3 times  $L_{\text{Edd}}$ .

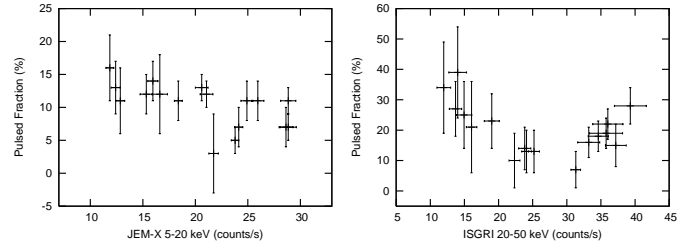


**Figure 10.** Plots of the *INTEGRAL* measurements of the pulsed fraction against total pulsed+unpulsed flux during the 2008 outburst of GRO J1750–27.

cause of the ambiguities in identifying the correct period, due to aliasing of the periodic signal, and the poor quality of the data caused by the background sources in the very large field of view. However, once these results are compared with the very high quality pulsation measurements from ISGRI it is very easy to see that the time evolution of the pulsar can be measured over a long time scale with BAT. This suggests that outbursts from other BeXRBs and other reasonably bright pulsars with periods  $>$  few seconds could be equally well measured and shows the power of having two complimentary instruments in *Swift* and *INTEGRAL* simultaneously operational. If a proper treatment of the background in the detector plan count-rate data led to an increase in sensitivity then it may be feasible to follow the pulsations from numerous objects, for example the large numbers of BeXRBs found in the Magellanic clouds.

## ACKNOWLEDGEMENTS

Based on observations with *INTEGRAL*, an ESA project with instruments and science data centre funded by ESA member states (especially the PI countries: Denmark, France, Germany, Italy, Switzerland, Spain), Czech Republic and Poland, and with the participation of Russia and the USA. *Swift*/BAT transient monitor results provided by the *Swift*/BAT team; particular thanks to H. Krimm for helpful support. 2–10 keV quick-look results provided by the ASM/RXTE team. SS’s work was conducted despite support from PPARC/STFC. JC acknowledges financial support from ESA-PRODEX 90057. The anonymous referee is thanked for a prompt response and helpful comments. A.J. Bird, V. McBride and T. Maccarone are also thanked for useful discussions.

## REFERENCES

- Barthelmy S. D., Barbier L. M., Cummings J. R., Fenimore E. E., Gehrels N., Hullinger D., Krimm H. A., Markwardt C. B., Palmer D. M., Parsons A., Sato G., Suzuki M., Takahashi T., Tashiro M., Tueller J., 2005, *Space Science Reviews*, 120, 143
- Barthelmy S. D., Baumgartner W. H., Brown P. J., Chester M. M., Cummings J. R., Gehrels N., Hoversten E. A., Kennea J. A., Palmer D. M., Parsons A. M., Racusin J. L., Sato G., Stroth M. C., vanden Berk D. E., 2008, *GRB Coordinates Network*, 7274, 1
- Bildsten L., Chakrabarty D., Chiu J., Finger M. H., Koh D. T., Nelson R. W., Prince T. A., Rubin B. C., Scott D. M., Stollberg M., Vaughan B. A., Wilson C. A., Wilson R. B., 1997, *ApJS*, 113, 367

- Bodaghee A., Courvoisier T. J.-L., Rodriguez J., Beckmann V., Produit N., Hannikainen D., Kuulkers E., Willis D. R., Wendt G., 2007, *A&A*, 467, 585
- Bretthorst G. L., 2001, in Mohammad-Djafari A., ed., *Bayesian Inference and Maximum Entropy Methods in Science and Engineering* Vol. 568 of American Institute of Physics Conference Series, Generalizing the Lomb-Scargle periodogram. pp 241–245
- Corbet R. H. D., 1986, *MNRAS*, 220, 1047
- Courvoisier T. J.-L., Walter R., Beckmann V., Dean A. J., Dubath P., Hudec R., Kretschmar P., Mereghetti S., Montmerle T., Mowlavi N., Paltani S., Zdziarski A. A., 2003, *A&A*, 411, L53
- Gehrels N., Chincarini G., Giommi P., Mason K. O., Nousek J. A., Wells A. A., White N. E., Barthelmy S. D., Burrows D. N., Cominsky L. R., 2004, *ApJ*, 611, 1005
- Ghosh P., Lamb F. K., 1979, *ApJ*, 234, 296
- Horne J. H., Baliunas S. L., 1986, *ApJ*, 302, 757
- Kreykenbohm I., Mowlavi N., Produit N., Soldi S., Walter R., Dubath P., Lubiński P., Türler M., Coburn W., Santangelo A., Rothschild R. E., Staubert R., 2005, *A&A*, 433, L45
- Krimm H. A., Barthelmy S. D., Cummings J., Fenimore E., Gehrels N., Markwardt C., Palmer D., Parsons A., Sakamoto T., Sato G., Skinner G., Stamatikos M., Tueller J., 2008, *The Astronomer's Telegram*, 1376, 1
- Kuulkers E., Beckmann V., Shaw S., Brandt S., Chenevez J., Courvoisier T. J.-L., Domingo A., Ebisawa K., Jonker P., Kretschmar P., Markwardt C., Oosterbroek T., Paizis A., Risquez D., Sanchez-Fernandez C., Wijnands R., 2008, *The Astronomer's Telegram*, 1385, 1
- Kuulkers E., Shaw S. E., Paizis A., Chenevez J., Brandt S., Courvoisier T. J.-L., Domingo A., Ebisawa K., Kretschmar P., Markwardt C. B., Mowlavi N., Oosterbroek T., Orr A., Risquez D., Sanchez-Fernandez C., Wijnands R., 2007, *A&A*, 466, 595
- Lebrun F., Leray J. P., Lavocat P., Crétolle J., Arquès M., Blondel C., Bonnin C., Bouère A., Cara C., Chaleil T., Daly F., Desages F., 2003, *A&A*, 411, L141
- Lomb N. R., 1976, *Ap&SS*, 39, 447
- Lund N., Budtz-Jørgensen C., Westergaard N. J., Brandt S., Rasmussen I. L., Hornstrup A., Oxborrow C. A., Chenevez J., Jensen P. A., Laursen S., Andersen K. H., Mogensen P. B., 2003, *A&A*, 411, L231
- Mowlavi N., Kreykenbohm I., Shaw S. E., Pottschmidt K., Wilms J., Rodriguez J., Produit N., Soldi S., Larsson S., Dubath P., 2006, *A&A*, 451, 187
- Porter J. M., Rivinius T., 2003, *PASP*, 115, 1153
- Pringle J. E., Rees M. J., 1972, *A&A*, 21, 1
- Russeil D., 2003, *A&A*, 397, 133
- Scargle J. D., 1982, *ApJ*, 263, 835
- Schönherr G., Wilms J., Kretschmar P., Kreykenbohm I., Santangelo A., Rothschild R. E., Coburn W., Staubert R., 2007, *A&A*, 472, 353
- Scott D. M., Finger M. H., Wilson R. B., Koh D. T., Prince T. A., Vaughan B. A., Chakrabarty D., 1997, *ApJ*, 488, 831
- Stella L., White N. E., Rosner R., 1986, *ApJ*, 308, 669
- Titarchuk L., 1994, *ApJ*, 434, 570
- Tsygankov S. S., Lutovinov A. A., Churazov E. M., Sunyaev R. A., 2006, *MNRAS*, 371, 19
- Ubertini P., Lebrun F., Di Cocco G., Bazzano A., Bird A. J., Broenstad K., Goldwurm A., La Rosa G., Labanti C., Laurent P., Mirabel I. F., Quadrini E. M., 2003, *A&A*, 411, L131
- Wang Y.-M., 1987, *A&A*, 183, 257
- Wang Y.-M., 1995, *ApJL*, 449, L153+
- Winkler C., Courvoisier T. J.-L., Di Cocco G., Gehrels N., Giménez A., Grebenev S., Hermsen W., Mas-Hesse J. M., Lebrun F., Lund N., Palumbo G. G. C., 2003, *A&A*, 411, L1
- Zombeck M., 2007, *Handbook of Space Astronomy and Astrophysics: Third Edition*. *Handbook of Space Astronomy and Astrophysics: Third Edition*, by Martin Zombeck. ISBN-10 0-521-78242-2 (HB); ISBN-13 978-0-521-78242-5 (HB). Published by Cambridge University Press, Cambridge, UK, 2007.